IMPULSIVE PHASE OF SOLAR FLARES I.

CHARACTERISTICS OF HIGH ENERGY ELECTRONS

by

John Leach

Vahé Petrosian

March 1981

National Aeronautics and Space Administration

Grant NSG 7092

Institute for Plasma Research
Stanford University
Stanford, California

IMPULSIVE PHASE OF SOLAR FLARES I.
CHARACTERISTICS OF HIGH ENERGY ELECTRONS

John Leach* and Vahé Petrosian*
Institute for Plasma Research
Stanford University
Stanford, CA

ABSTRACT

In this, the first of a series of papers, we investigate the variation along a magnetic field line of the energy and pitch angle distribution of high energy electrons injected into a cold hydrogen plasma containing either an open or closed magnetic field structure. The problem is formulated as a time-independent Fokker-Planck Equation for the electron number distribution as a function of the electron energy, electron pitch angle and the structure of the global magnetic field.

We present a simple analytic solution valid in the small pitch angle regime and for a slowly varying magnetic field. For the more general situation we use a numerical code for solving the Fokker-Planck Equation, and we find that the analytic expression agrees well with the numerical results to values of the pitch angle much larger than expected. For most practical applications one may confidently use the analytic expression instead of having to resort to lengthy numerical computations.

These results may be useful for a variety of astrophysical applications. Our primary concern is to use these results to study the non-thermal models of the impulsive phase of solar flares. In subsequent papers we shall use the results of this paper to calculate the expected x-ray and microwave radiation from a flaring loop and compare these results with the high resolution data currently becoming available.

Subject Headings: Atomic Processes, Sun: Flares, Sun: X-rays, Sun:Radio Radiation

*Also Department of Applied Physics

I. INTRODUCTION

Hard x-rays and microwave radiation observed during the impulsive phase of a solar flare provide us with a means for inferring the characteristics of the distribution of energetic electrons within the flaring plasma. Although it is now widely accepted that the hard x-rays and microwaves are the result of coulomb bremsstrahlung and gyrosynchrotron mechanisms respectively, there is still no consensus as to the form of the electron distribution function within the flaring loop nor as to the relative importance of the various candidate processes which may affect or determine the characteristics of this distribution.

Various models describing the operative physical processes have been proposed, broadly classified as thermal or non-thermal models (see Emslie and Rust 1979 and references therein). The non-thermal models may be subdivided into thick or thin target beamed electron models and trapped electron models. The prime differences between these models have often been taken to lie with the spectral distribution of accelerated electrons and the characteristics of the background plasma. (For a discussion of these models the interested reader is referred to Sturrock 1980, p. 215, and to Brown and Smith 1980).

Principally two types of mechanism have been suggested by which a situation giving rise to the emission of thermal hard x-ray bremsstrahlung from a flare may be obtained. What is required is the bulk heating of the loop plasma to a temperature of $\approx 10^8$ K as suggested by Chubb, Kreplin and Friedman (1966) to explain their early observations of hard x-rays of energies 20 keV and above.

One type of mechanism suggested by Matzler et al (1978) involves the reversible adiabatic compression and heating of the plasma. There are, however, both observational and theoretical problems with this model (see Elcan 1980). Another type of mechanism is to accelerate electrons to high energies in the

reconnection region and to inject these electrons as a high current beam into the ambient flare plasma of low density. Plasma-beam instabilities generate turbulence (ion-cyclotron or ion-acoustic, Kendell and Kennel 1971, also Duijveman, Hoyng and Ionson 1981; Emslie 1981b) which enhances the electrical resistivity of the plasma and rapidly dissipates the electron beam depositing the beam energy as heat in the ambient plasma. The development of thermal models has been previously discussed (e.g., Brown, Melrose and Spicer 1979; Smith and Lilliequist 1979; Smith and Auer 1980; Emslie 1981a) and we shall not concern ourselves with such models here.

The purpose of this series of papers is to analyze the general characteristics of the "non-thermal" models. All previous analyses of these models (e.g., Ramaty and Lingenfelter 1967; Lin and Hudson 1971; Brown 1972; Takakura 1972; Petrosian 1973; Kane 1974) have been limited to total flux calculations and have either ignored the dispersion in phase space of the accelerated electrons or treated such in an approximate manner. The high spatial resolution capabilities of the HXIS experiment on the SMM and various on-going observational programs using the VLA and other high resolution microwave instruments will soon provide us with detailed hard x-ray images and microwave maps of flares during the impulsive phase. In order to utilize these observations we need to evaluate the distribution of high energy electrons along the flare loop and calculate the resultant x-ray and microwave radiation as a function of position along the loop.

In this paper we present the results of our analysis on the steady state distribution of energetic electrons within the flare plasma. We use the time independent Fokker-Planck equation to determine the steady state distribution in pitch angle, energy and height above the photosphere of the electrons as they spiral along the magnetic field lines and collide with the particles in the ambient plasma. In subsequent papers this distribution will be used to calculate the characteristics of the resultant x-ray and microwave radiation. In §II

we present the general features of this problem and the equations to be used in its solution. Some approximate analytic solutions are discussed in §III, and the results of the numerical analysis are presented in §IV. In §V we present a summary and our conclusions.

II. THE MODEL

The model we are investigating, which encompasses thick-target, thin-target and trap aspects of non-thermal hard x-ray models, is the following: High energy electrons with some initial energy spectrum and pitch angle distribution are injected at some height above the photosphere either into a closed magnetic loop structure or into an open field structure (see Figure 1). These electrons, spiraling along the field lines, undergo collisions with the background particles (atoms, ions and electrons) and these collisions, in addition to the variations in the magnetic field structure, diffuse the energetic electrons' distribution function in phase space. Note that wave-particle interactions, which may be important under certain circumstances, are not dealt with in this paper. In order to calculate the radiation from the electrons, we must first evaluate the distribution in phase space of the electrons.

Two characteristics of the background plasma simplify this calculation significantly.

a) The time scale for energy loss by collisions is

$$\tau_{coll} = E/\dot{E}_{coll} \approx E\beta/4\pi r_o^2\, n c \ln\Lambda \qquad (1)$$

where $E = \gamma - 1$ is the electron kinetic energy in units[1] of $m_e c^2$, $\beta^2 = 1 - 1/\gamma^2$,

---

[1] All energies will be expressed in these units unless otherwise specified.

$4\pi r_o^2 = 10^{-24}\,cm^2$, and Λ^{-1} is the minimum angle of deflection in the couloumb integral, typically $\ln\Lambda \approx 20$. At a density of $10^{10}\,cm^{-3}$ $\tau_{coll} \leq 1$ sec for electrons with energy < 10 keV and is correspondingly longer for higher energy electrons. However, since the time $L/\beta c$ for electrons to traverse a typical magnetic loop ($L \leq 10^{10}$ cm) is less than a second, the more energetic electrons penetrate the high density regions and lose energy within less than a second

(cf. Petrosian 1973). It then follows that for the study of the impulsive phase on time scales longer than this the electrons can be treated as if in steady state.

b) For electrons with energies 10 to 1000 keV the gyro radius, $r_B \approx 10$ (100 gauss/B) cm, is much shorter than the characteristic length scales of the plasma, namely, the density or magnetic field scale heights, which are of the order of $L \approx 10^9$cm. Consequently, electrons on different field lines are decoupled and the diffusion of the electrons perpendicular to the magnetic field can be ignored. Thus, the electron distribution varies only along the magnetic field lines, which we take to be static.

With these considerations the problem is reduced to a three dimensional time independent diffusion problem: One spatial dimension s along the field line and two momenta (parallel and perpendicular to the field lines respectively). It is more convenient to use as independent variables the cosine of the electron pitch angle, $\mu = \hat{p}\cdot\hat{b}$ ($\hat{p}$ and $\hat{B}$ are unit vectors in the direction of the electron momentum and the downward magnetic field), the electron kinetic energy E and a dimensionless column depth τ defined by

$$d\tau = ds/\lambda_o, \quad \lambda_o^{-1} = 4\pi r_o^2 \, n \, \ln\Lambda = 2 \times 10^{-13}\text{cm}^{-1}(10^{10}\text{cm}^{-3}/n)(\ln\Lambda/20) , \qquad (2)$$

where n is the number density of hydrogen and λ_o is a mean free path scale (the mean free path for electrons of energy E is $\lambda_o E\beta^2$). Note that for $\ln\Lambda = 20$, $\tau = 1$ corresponds to a column depth of $5 \times 10^{22}\text{cm}^{-2}$ which, in the quiet sun, is approximately where the temperature minimum is to be found.

We use the Fokker-Planck method to solve for the diffusion in pitch angle and energy along a field line of given geometry and field strength. Let $f(E,\mu,\tau)dEd\mu d\tau$ be the number density of electrons with cosine of pitch angle between μ and $\mu + d\mu$, and with kinetic energy between E and $E + dE$, lying between

column depths τ and $\tau + d\tau$. The Fokker-Planck equation for the problem becomes (see e.g., Rosenbluth, McDonald and Judd 1957)

$$\mu\frac{\partial f}{\partial \tau} = (1-\mu^2)\,\frac{d\ln B}{2d\tau}\,\frac{\partial f}{\partial \mu} + \frac{C_1}{\beta}\,\frac{\partial}{\partial E}\left(\frac{f}{\beta}\right) + \frac{C_2}{\beta^4\gamma^2}\,\frac{\partial}{\partial \mu}\left[(1-\mu^2)\,\frac{\partial f}{\partial \mu}\right] , \qquad (3)$$

where we have ignored terms in the Fokker-Planck expansion which do not contain the large $\ln\Lambda$ coefficient. The first term on the right hand side describes the mirroring of the particles owing to the convergence of the magnetic field. The last two terms account for the energy loss and pitch angle dispersion of the beam through collisions with the ambient particles. The coefficients C_1 preceding the energy dissipation term and C_2 preceding the pitch angle diffusion term depend upon the composition of the plasma. For a partially ionized plasma where $x = n_e/n$ is the fraction of the hydrogen that is ionized

$$C_1 = x + \frac{(1-x)}{2}\,\frac{\ln(\beta^2\gamma^2 E/\alpha^4)}{\ln\Lambda} , \qquad C_2 = \tfrac{1}{2} + \frac{(1+\gamma)}{4}\,C_1 , \qquad (4)$$

where α is the fine structure constant ($\frac{1}{2}\alpha^2$ is the ionization potential for hydrogen in units of $m_e c^2$). For a fully ionized plasma $x = 1$ and the coefficients C_1 and C_2 reduce to

$$C_1 = 1, \quad C_2 = \frac{3+\gamma}{4} , \qquad (5)$$

so that, for non-relativistic electrons, $C_2 = C_1$.

Other than hydrogen the solar atmosphere contains only helium in significant quantities. For a helium fraction, by number, of 10%, the helium's

contribution to each of the coefficients C_1 and C_2 is limited to $C_1^{He} \leq C_1^H/5$, $C_2^{He} \leq C_2^H/3$. We shall ignore the slight differences between the relative contributions of helium to C_1 and C_2 and shall absorb this 20 to 30 percent contribution from helium into the uncertainties in the values of $\ln\Lambda$ and the density n. Therefore, we consider a pure hydrogen atmosphere.

We have neglected the energy losses of the electrons due to the electric field needed to drive the reverse current, an assumption which holds well for high density and temperature plasmas and for small fluxes of accelerated electrons (cf. Knight and Sturrock 1977; Emslie 1980). The contribution of the energy loss due to the reverse current electric field can also be included in the above equation. However, this will complicate the solution considerably since the strength of the electric field at each level depends on the total flux of electrons at that depth $F(\tau) = \int\int \mu\beta c f(E,\mu,\tau) dE d\mu$, so that instead of a single differential equation we would have to consider a coupled integro-differential equation. This is beyond the scope of the present paper and will be considered in future work.

In the next two sections we discuss some approximate analytic and some accurate numerical solutions of equation (3).

III. SOME ANALYTIC SOLUTIONS

In order to solve equation (3) we need to specify the characteristics of the plasma which determine the parameters C_1, C_2 and $d\ln B/d\tau$, and the boundary conditions. We assume that particles are injected at the top of the loop ($\tau = 0$), such that the spectrum at $\tau = 0$, $f_o(E,\mu)$ is specified for $0 < \mu \leq 1$, the other boundary condition being that $f(E,\mu,\tau\to\infty) = 0$. (The coefficients C_1 and C_2 are approximately unity and have only a slight energy dependence.) The parameter $d\ln B/d\tau$ describes the variation of the magnetic field and determines its influence on the electron beam according to the first term on the right hand side of equation (3). If the magnetic field and the density variation can be described by scale heights H_B and H_n, viz, $n = n_o \exp(s/H_n)$; $B = B_o \exp(s/H_B)$, then, in terms of our column depth τ we find $d\ln B/d\tau = \lambda_o/H_B = H_n/\tau H_B$. Clearly when $H_n/H_B \ll 1$ (i.e., when the B field is nearly uniform while the density varies rapidly) the magnetic field has an insignificant effect and the electron distribution is modified by collisions alone. The resulting model is a thick target model with the degree of beaming determined by the injected spectrum. In the other extreme case, when $H_n/H_B \gg 1$ (i.e., low and nearly uniform plasma density and rapid field variation) the particles are reflected back and forth between mirror points of a closed loop configuration leading to a trap model with slow rate of precipitation, unless the density, n_o, is so high that the mirror points occur at $\tau \gtrsim 1$. For an open field line configuration, particles are reflected no more than once and escape along the diverging field lines, giving rise to a situation as described by a thin target model (Datlowe and Lin 1973). However, it is usually found that the situation is more complicated owing to the variation of $d\ln B/d\tau$ along the field lines.

In general, equation (3) cannot be solved analytically, and in the next section we shall describe a procedure for its numerical solution. Here we shall consider some special cases which allow us to derive exact analytic results.

The purpose of this is to check the accuracy of the numerical results and to derive some scaling laws which may simplify the presentation of those results.

Case 1: If the plasma density is low and the magnetic field scale height H_B is much smaller than the density scale height H_n (so that $d\ln B/d\tau = \lambda_0/H_B >> 1$ throughout), then the last two terms on the right-hand side of equation (3) are negligible ($C_1=C_2=0$), and we have a situation corresponding to a collisionless trap model. It is then easy to show that the distribution function satisfies the differential equation

$$\partial f/\partial\bar{\tau} = -\partial f/\partial \ln(1-\mu^2), \quad \bar{\tau} = \int_0^{\tau} \frac{d\ln B}{d\tau}\, d\tau = \ln \frac{B(\tau)}{B(0)} \quad , \tag{6}$$

giving a distribution function which is independent of energy and has the form

$$f(\tau,\mu) = f_0\{[1-(1-\mu^2)e^{-\bar{\tau}}]^{\frac{1}{2}}\} \quad , \tag{7}$$

where $f_0(\mu)$ is the injected pitch angle distribution at $\tau = 0$. This is simply a description of the adiabatic invariance of $B/(1-\mu^2)$. Note that for an isotropic injected pitch angle distribution $f_0(\mu)$ is independent of μ and the pitch angle distribution remains isotropic throughout the atmosphere. For a gaussian injected distribution the distribution remains gaussian but with a width that increases with $\bar{\tau}$.

Case 2: If the magnetic field is approximately uniform such that $H_B >> H_n$ and λ_0, then the first term on the right-hand side of equation (3) is negligible. However, even when $d\ln B/d\tau = 0$, analytic solutions cannot be obtained except in the small pitch angle [$(1-\mu) << 1$] regime. Before presenting the solution for the general small pitch case, we first consider the following two cases, which, though unphysical, expose the nature of the results for the physical case and which may be used for testing the numerical code (see Appendix).

a) Energy loss term with no pitch angle scattering ($C_1 = 1$, $C_2 = 0$, $d\ln B/d\tau = 0$). In this case it is useful to define

$$\phi \equiv f/\beta, \quad d\eta \equiv \beta^2 dE, \quad \eta \equiv E^2/(E+1) \tag{8}$$

so that for a given (and constant) pitch angle μ equation (3) and its solutions are

$$\frac{\partial\phi}{\partial\tau} = \frac{\partial\phi}{\partial\eta} \Rightarrow \phi(\mu,\eta,\tau) = \phi_0(\frac{\tau}{\mu} + \eta) \ , \tag{9}$$

where $\phi_0(\eta)$ is related to the injected spectrum $f_0(E)$ through definitions (8). For non-relativistic energies $\eta \propto E^2 \propto \beta^4/4$, and

$$f(E,\mu,\tau) = f_0(E\sqrt{1+\tau/\mu E^2}) \cdot (1+\tau/E^2)^{-\frac{1}{2}} \ . \tag{10}$$

(b) Pitch angle diffusion with no energy degradation ($C_1=0$, $C_2 = \frac{3+\gamma}{4}$, $d\ln B/d\tau = 0$). In this case analytic solutions are possible only for small pitch angles. If we define

$$\alpha^2/2 \equiv 1 - \mu << 1 \quad \text{and} \quad \bar{\tau} = C_2\tau/\beta^4\gamma^2 \ , \tag{11}$$

where α is approximately equal to the pitch angle, then the differential equation (3) reduces to

$$\frac{\partial f}{\partial\bar{\tau}} = \frac{1}{\alpha}\ \frac{\partial}{\partial\alpha}\left(\alpha\ \frac{\partial f}{\partial\alpha}\right) \ ,$$

which has the solution

$$f(\tau,\alpha) = \int_0^\infty e^{-\omega^2\bar{\tau}} A(\omega)\ J_0(\omega\alpha)d\omega \ , \tag{12}$$

where J_0 is the Bessel function of order zero and $A(\omega)$ is determined by the boundary conditions. For example, if the injected pitch angle distribution is gaussian, $f_0(\alpha) = (\frac{2}{\alpha_0^2})e^{-\alpha^2/\alpha_0^2}$ with $\alpha_0^2 << 1$, then multiplication of both sides of equation (12) by $J_0(\omega\ \alpha)$ and integration over all α for $\tau = 0$ gives

$$A(\omega')/\omega' = \int_0^\infty f_0(\alpha) J_0(\omega'\alpha)\alpha d\alpha = e^{-[(\omega'\alpha_o/2)^2]} . \tag{13}$$

Substituting this into equation (12) we obtain

$$f(E,\mu,\tau) = \left(\frac{2}{\alpha_o^2+4\tau}\right) \exp\left\{-\frac{\alpha^2}{\alpha_o^2+4\tau}\right\} \tag{14}$$

c) The general small pitch angle case with a uniform magnetic field ($C_1 = 1$, $C_2 = \frac{3+\gamma}{4}$, $\frac{d\ln B}{d\tau} = 0$). In this case we have again $\alpha^2/2 = (1-\mu) << 1$ so that with the help of definition (8) equation (3) is reduced to

$$\frac{4\beta'\gamma^2}{3+\gamma}\left(\frac{\partial\phi}{\partial\tau} - \frac{\partial\phi}{\partial\eta}\right) = \frac{1}{\alpha}\frac{\partial}{\partial\alpha}\left(\alpha\frac{\partial\phi}{\partial\alpha}\right) \tag{15}$$

which has the general solution (separable in τ,η and α).

$$\phi(\tau,\eta,\alpha) = \int_0^\infty e^{-\lambda\tau} e^{-\lambda\eta} B(\lambda) d\lambda \int_0^\infty [\xi(\eta)]^{\omega^2} J_0(\omega\alpha) A(\omega) d\omega , \tag{16}$$

where

$$\xi(\eta) = \exp\left\{\int^\eta \frac{C_2}{\beta'\gamma^2} d\eta\right\} = \left(\frac{E^2(\eta)}{2+E(\eta)}\right)^{1/4} \tag{17}$$

and $B(\lambda)$ and $A(\omega)$ are determined from the boundary conditions. For an injected gaussian pitch angle distribution $f(E,\mu,\tau = 0) = f_0(E)(2/\alpha_o^2)e^{-\alpha^2/\alpha_o^2}$, where $\alpha_o^2 << 1$, from equation (8) we can obtain an expression for $\phi_o(\eta) = f_0[E(\eta)]/\beta(\eta)$. Then, following procedures similar to those in deriving equations (9) and (14), equation (16) generates

$$f(E,\mu,\tau) = f_0(\eta+\tau)\frac{\beta(\eta)}{\beta(\eta+\tau)} \frac{2}{\alpha_o^2 + \ln\zeta} \exp\left\{-\frac{\alpha^2}{\alpha_o^2 + \ln\zeta}\right\} ,$$
$$\cdot\ \zeta \equiv [\xi(\eta+\tau)/\xi(\eta)]^4 . \tag{18}$$

In the non-relativistic limit $\xi(\eta) \propto \eta^{\frac{1}{4}} \propto E^{\frac{1}{2}} \propto \beta/\sqrt{2}$ and equation (18) becomes

$$f(E,\mu,\tau) = f_0(\zeta^{\frac{1}{2}}E)\zeta^{-\frac{1}{4}}[2/(\alpha_0^2 + \ln\zeta)]e^{-[\alpha^2/(\alpha_0^2+\ln\zeta)]} \quad , \tag{19}$$

$$\zeta \simeq (1 + \tau/E^2).$$

It is normally more convenient to use the flux of particles, $F(E,\mu,\tau)$, instead of their number density, $f(E,\mu,\tau)$, where the flux and number density are related by $F(E,\mu,\tau) = c\beta f(E,\mu,\tau)$. The relationship between $F(E,\mu,\tau)$ and the injected flux at $\tau = 0$, $F_0(E,\mu)$ is similar to the relationship between $f(E,\mu,\tau)$ and $f_0(E,\mu)$ as given in equations (18) and (19), these relationships being obtained by replacing f and f_0 by F and F_0 and by changing $\beta(\eta)/\beta(\eta+\tau)$ to $[\beta(\eta)/\beta(\eta+\tau)]^2$ in equation (18) and $\zeta^{-\frac{1}{4}}$ to $\zeta^{-\frac{1}{2}}$ in equation (19).

As is evident, the shapes of the pitch angle distributions at various τ are identical provided the scaling parameter ζ is constant. Similarly, for an injected power law flux spectrum $F_0(E) \propto E^{-\delta}$, the ratio of the energy spectra at various depths τ to the injected spectrum have the same shape for constant values of ζ. In the next section we shall explore the extent to which this scaling law holds for large pitch angles and for non-uniform magnetic field configurations.

IV. NUMERICAL RESULTS

We have solved equation (3) numerically using a modified version of the program developed by Walt et al (1968) for the related problem of auroral electrons (see also Walt 1967). For a prescribed injection spectrum $f(E,\mu)$ at $\tau = 0$, the program solves for $f(E,\mu,\tau)$ for $\tau > 0$, utilizing either a reflecting or non-reflecting boundary condition at the top of the atmosphere ($\tau = 0$), thereby calculating the electron distribution function for a closed or open field line configuration respectively (see below). The details of the procedure are described in the appendix along with the results of our testing the numerical code against the analytic results described in the previous section. We now present some numerical results for the electron distribution function for the nine models described in Table 1. We use model 1 as our standard model and as a basis for comparison so that we may observe the effects of the parameters describing the ambient plasma, the magnetic field configuration and the injected spectrum on the electron distribution function.

Model 1 has an injected electron spectrum

$$F(E,\mu>0,\tau=0) = F_0(E,\mu) = A\left(\frac{E}{E_0}\right)^{-\delta} \exp-\left\{\frac{1-\mu^2}{\alpha_0^2}\right\} , \qquad (20)$$

with $\alpha_0^2 = 0.01$ and $\delta = 5$ (a typical value from solar hard x-ray bursts), a fully ionized hydrogen atmosphere with a uniform vertical magnetic field and an open, i.e. non-reflecting, boundary condition at the top. This means that electrons which return to $\tau = 0$ and therefore have pitch angle cosines $\mu < 0$ are allowed to exit from the top of the atmosphere and are lost from the calculation. In Figure 2 we show the evolution of the electron flux with depth as a function of pitch angle for this model. The evolution of the flux distribution is similar for different energies provided

the depth τ is suitably scaled. For all except the highest energies, that is, at non-relativistic energies, the scaling expressed by the numerical results is the scaling $\tau \propto E^2$, [see equation (19) with ζ = constant]. Consequently, the curves in Figure 2 are labelled according to their value of the parameter τ/E^2. This scaling of $\tau \propto E^2$ is to be expected as the electron mean free path is proportional to the square of the electron energy for non-relativistic energies. Near to the top of the atmosphere most of the electrons of a particular energy E were originally electrons injected at $\tau = 0$ with an energy slightly in excess of E and which have lost only a small fraction of their energy and which have been deflected only slightly away from their original pitch angle. As can be seen, the forward beam of electrons is still clearly defined and only slightly broader than the beam at injection. These curves also show that, even at small τ/E^2, there is an, albeit negligible, component to the flux of electrons with $\mu < 0$. This effect is due to those few electrons which, despite the extremely low probability of being scattered through very large angles of the order of π, have been scattered within the atmosphere sufficiently that they have returned towards the top of the atmosphere. In the process they have also lost a substantial amount of energy, indicating that these electrons originally possessed energies considerably higher than E and were, therefore, injected in fewer number [see equation (20)].

At successively deeper levels in the atmosphere, i.e., at larger values of τ/E^2, the flux distribution as a function of pitch angle becomes increasingly more uniform and the forward beam broadens, reflecting the fact that at great depths the number of electrons with kinetic energy E to be found at any pitch angle comprises a very broad range of electrons injected at the top of the atmosphere with many different energies and with many different pitch angles.

At greater depths still, the total number of electrons at any energy falls (as is to be expected), but the beam is still well defined.

The scaling described by equation (19), which was obtained from the small pitch angle approximation, appears to be valid through to much larger pitch angles. It breaks down at higher energies due to increasing relativistic effects ($\zeta \neq 1 + \tau/E^2$) and the fact that our injected spectrum has an arbitrarily imposed cutoff at an electron kinetic energy of 1 MeV. We also find that, in agreement with equations (18) and (19), the curves in Figure 2 may be approximated by gaussians to a good degree of accuracy even out to large pitch angles where the flux ratios have dropped to insignificant levels (a fraction of one percent of the forward, [$\mu = 1$], fluxes). The widths of these gaussians also agree with those expected from equation (19) as shown by the inset in Figure 2 where the analytic gaussians (solid lines) are compared to the numerical values (points).

In Figure 3 we show the energy spectrum at various depths for model 1, with the ordinate being the integrated electron flux in the forward direction. At the top of the atmosphere the energy spectrum is the injected spectrum, $E^{-\delta}$. However, as the beam moves through the atmosphere, the lower energy electrons lose energy more rapidly than the higher energy electrons and soon their numbers become depleted, giving rise to the humped spectrum that forms throughout the atmosphere.

Integration of equation (18) over pitch angle, $d\mu = \alpha d\alpha$, yields, using the electron flux $F(\tau,E)$ rather than the electron density $f(\tau,E)$,

$$F(\tau,E) = \left(\frac{\beta(\eta)}{\beta(\eta+\tau)}\right)^2 F_0(\eta+\tau) = F_0(\zeta^{\frac{1}{2}}E)/\zeta^{\frac{1}{2}} \quad , \qquad (21)$$

which implies that, in the non-relativistic limit and for a power law injected electron spectrum $F_0(E) \propto E^{-\delta}$, the maxima of the above curves occur at $E^2_{max} = \tau/\delta$. As

shown by the inset in Figure 3 this relationship holds well for numerical results.

Furthermore, at non-relativistic energies and for a power law injected spectrum, the flux in the forward direction normalized to that at the top,

$$F(\tau,E,\mu=1)/F_0(E,\mu=1) \approx \zeta^{-(\frac{\delta+1}{2})} / (1+\alpha_0^{-2}\ln\zeta) \quad , \qquad (22)$$

depends only on the parameter ζ. Figure 4 compares the values of this ratio with the values obtained from the numerical calculations. For 30 keV and 70 keV electrons the agreement is excellent for the range of values of the parameter ζ pertinent to solar flares. For 750 keV electrons we also compare the numerical results with the fully relativistic form of equation (18) and present this in the upper of the two curves for 750 keV. It is evident that the relativistic form indeed becomes necessary at high energies. Note that the analytic expression begins to deviate significantly (>20%) only at depths $\tau/E^2 > 0.3$ where the electron flux is less than one percent of the injected flux (see Figure 2). Figures similar to Figures 3 and 4 may be drawn for the flux at any particular forward pitch angle but, given the good agreement between the results and the analysis as displayed in Figure 2, those figures obtained would clearly be very similar to Figures 3 and 4 which have been drawn using the integrated forward flux.

Finally, if we integrate the above spectra over all depths, we obtain the spatially-integrated energy spectrum (which determines the radiation spectrum of the whole, unresolved loop).

$$F(E) = \int_0^\infty \Gamma(\tau,E)d\tau = \int_0^\infty \left(\frac{\beta(\eta)}{\beta(\eta+\tau)}\right)^2 F_0(\eta+\tau)d\tau = \beta^2(\eta)\int_E^\infty F_0(E')dE' \qquad (23)$$

which, for $F_o(E) \propto E^{-\delta}$

$$F(E) \propto E^{-\delta+1}\beta^2 \approx E^{-\delta+2}\left(1 - \frac{3E}{2} + \text{----}\right) \qquad (24)$$

Note that this result is not restricted to the small pitch angle regime. This can be demonstrated by integrating equation (3) first over μ and then over τ which gives

$$\frac{d}{dE}\left(\frac{F(E)}{\beta^2}\right) = F_o(E)\,\overline{\mu(o)} \quad , \quad \overline{\mu(\tau)} = \int_{-1}^{+1} \mu F(E,\mu,\tau)d\mu \Big/ \int_{-1}^{+1} F(E,\mu,\tau)d\mu \ . \qquad (25)$$

Integration of this gives equation (23) which was derived from the special case of $\overline{\mu(o)} \approx 1$. .

In Figure 5 we plot F(E) versus E for model 1 showing an agreement between our results and the above relationship which is especially good at low energies. This agreement breaks down at higher energies for two reasons: (i) $F(E) \to E^{-\delta+1}$ at extreme relativistic energies, and (2) the presence of an upper cutoff in the energy of the injected beam.

Also shown in Figure 5 is the same function for models 5 and 9, both of which display a similarly good agreement with the analysis. Model 5 has a value of $\delta = 3$, and model 9 is, parametrically, most distant from model 1 and from the approximations used in the analysis of model 1.

In summary, the excellent agreement between our numerical results and the above analysis of model 1, in addition to providing us with ample demonstration of the accuracy of the numerical results, indicates that the analytic results hold to a high degree of accuracy well outside the regimes of validity suggested

by the approximations used (that is, to large pitch angles) and that the analysis provides a good description of the evolution of the electron beam throughout the atmosphere.

Results for Other Models

We now consider the results from the other models described in Table 1 and compare them with those from model 1.

Model 2 has a strongly converging magnetic field throughout the atmosphere but retains the open boundary condition at $\tau = 0$. The effect of the converging magnetic field is to enhance the broadening of the pitch angle distribution with depth and to increase significantly the number of electrons which are moved to negative pitch angle cosines and return towards the top of the atmosphere. However, despite the presence of the magnetic field which converges by a factor of roughly thirty from $\tau = 0$ to $\tau \simeq 1$, the narrowness of the injected pitch angle spectrum is such that the downward traveling electron beam contains about two orders of magnitude more electrons than are removed from the beam by the magnetic mirroring so that the beam stays well defined throughout the atmosphere.

Model 3 is as model 2 but investigates the effects of reflecting those electrons with $\mu < 0$ at $\tau = 0$ back into the loop with $\mu > 0$. This mimics the effects of having the electrons in a closed and symmetric loop configuration (see Fig. 1). However, since the number of electrons exiting with $\mu < 0$ is relatively small, the effects of this change on the boundary condition at $\tau = 0$ is negligible.

Model 4 is the same as model 1 except that it has an atmosphere which is fully ionized down to a column depth of $5 \times 10^{19} cm^{-2}$ and then becomes fully neutral as rapidly as can be handled by the numerical code and assumes chromospheric densities throughout the remaining depths. Thus, model 4 introduces a transition region and has changing

values of the parameters C_1 and C_2 [see equation (4)]. The effects, however, on the overall electron distribution, of having a partially ionized atmosphere, are small with the beam being only slightly affected below the transition region (cf. Emslie 1978).

Figure 3 shows the energy spectrum as a function of depth for model 1. A similar plot for models 2 through 4 shows that the energy spectrum at each depth is almost completely insensitive to the changes in the parameters introduced with these models and the humped spectrum is maintained with the same scaling $E^2_{max} \propto \tau$. This is as expected because models 2 through 4 remain primarily collisional in their treatment of the beam despite the introduction of the converging magnetic field, etc., and therefore exhibit the same scaling as model 1.

In general, we therefore conclude that for a narrow injected pitch angle distribution the change in the plasma parameters and the introduction of a reasonable magnetic field configuration have a negligible effect on the evolution of the electron beam within the upper part of the target and tend to make the electron flux more uniform in the lower parts where the beam flux is less than 0.1% of the injected beam flux.

Model 5 is identical to model 1 but has a harder electron energy spectrum with $\delta = 3$ (corresponding to the hardest observed x-ray spectra) in place of $\delta = 5$. Having more high energy electrons in the beam at the top of the atmosphere simply leads to having more electrons with medium energy at large pitch angles lower in the atmosphere and a larger number of electrons reflected back upwards with $\mu < 0$. Otherwise this model, like model 1, agrees well with the analytic expression given by equation (19) indicated, for example, in Figure 5.

Model 6 has a much broader injected gaussian pitch angle distribution; $\alpha_o^2 = 0.125$. In Figure 6 we show the evolution of the electron flux distribution for this model where, comparing Figure 6 with Figure 2, we can see that the

effect of having a broader injected beam is solely to give rise to a broader beam traveling downwards through the upper atmosphere. However, the shape of the flux distribution at greater depths becomes identical to the shape of the distribution function at the same depths in Figure 2. Remembering that the curves in Figures 2 and 6 give the beam evolution with τ scaling as E^2, we can see that for each energy there is a depth below which the shape of the distribution function in pitch angle is independent of the injected gaussian width. This is to be expected from equation (18) owing to the fact that $\ln\zeta$ increases slowly with τ until it eventually overwhelms α_o^2 even for the broad injected beam. Thus, below a certain depth the electron flux distribution relaxes to a smooth form and then slowly isotropizes. Only at exceptionally large depths where the electron flux is negligible does the distribution become sufficiently isotropic that the forward component is not easily discernable. The inset in Figure 6 is similar to that in Figure 2 and shows the extent to which the small pitch angle approximation agrees with the numerical results for this model. Considering that the injected spectrum is broad, this agreement is better than might have been expected, the agreement holding well out to large pitch angles.

Model 7 is the same as model 1 with the exception of now having an injected pitch angle spectrum which is uniform for positive μ. The evolution of the pitch angle spectrum with depth is shown in Figure 7 and again we see that the shape of the spectrum at the two greatest depths is nearly identical to those in Figures 2 and 6 despite the extreme form of the injected spectrum.

In models 8 and 9 the magnetic field is non-uniform (as in models 2 and 3) but with an injected spectrum which is uniform as in model 7. In addition, model 9 has a reflecting boundary at the top. Little needs to be remarked upon for models 8 and 9 other than that, as expected, the effects of the vertical converging magnetic field and the reflecting boundary condition are to give almost a symmetric

pitch angle distribution with $f(\mu) \approx f(-\mu)$ at each depth, the discrepancy being the leakage of electrons to lower energies by collisions. For comparison with Figure 3 the energy spectrum evolution with depth of model 9 is shown in Figure 8. It can be seen that, even for model 9 which is parametrically most distinct from model 1, the energy spectrum retains the same form with the peak in the spectrum moving to higher energies with increasing depth in accordance with $\tau \propto E_{max}^{2}$ as shown in the inset.

V. SUMMARY AND CONCLUSIONS

1. If the injected spectrum is strongly concentrated in the direction of the magnetic field lines (small pitch angles), plausible variations in the parameters describing the plasma and the field configuration have significant effects only at large depths and large pitch angles where the beam density has fallen by several orders of magnitude. Otherwise, the analytic results of equations (18) and (19) give an acceptably accurate description of the evolution of the beam.

2. Even when the injected electrons are weakly beamed or not beamed at all (uniform pitch angle distribution), the scaling derived from the small pitch angle regime seems to be valid except at small optical depths (see Figures 6 and 7).

3. At large depths the pitch angle distribution is independent of the injected distribution, evolving to a smooth and broad distribution.

4. The energy spectrum evolves independently of the injected pitch angle distribution and agrees quite well with the analytic approximation given by equation (21).

5. Most significantly we find that for most practical applications equations (18) to (24) may be used instead of having to resort to detailed numerical calculations.

In future papers in this series we intend to utilize the results discussed and described here to calculate the radiation observed from a flaring loop. Using the complete electron flux distribution, we will be able to calculate the polarization and directivity of hard x-rays from the loop, the hard x-ray flux as a function of position along the loop and the details of the microwave flux including its dependence on the magnetic field structure defining the loop.

With results from current observational programs at the VLA (Marsh et al 1980) and the high resolution data from HXIS (Hoyng et al 1981), to mention but two of the many sources of high quality observational data, we hope to be able to use our results as a powerful diagnostic tool for the further understanding of the impulsive phase of flares.

The model as it stands has several limitations which will receive attention in the future pursuit of this work. The effects of reverse currents may, under certain physical conditions of the ambient plasma (see Emslie 1980, 1981b), be of significance in determining the evolution of the flux of accelerated electrons in a flare limb and are intended to be included in the model to give it greater applicability for a broader range of flare parameters. Similarly, the effects of wave particle interactions on the energy spectrum at energies below that of maximum flux will also be investigated.

APPENDIX

A. Description of the Numerical Code

We consider a (horizontally uniform) 1-dimensional plasma atmosphere with a density structure corresponding approximately to the low corona and chromosphere and inject electrons at the top of the atmosphere, designated as $\tau = 0$.

The electrons are injected according to a prescribed pitch angle distribution with the electron's pitch angle being measured as the angle between the electron's instantaneous velocity vector and the magnetic field line which is in the downward direction along a flare loop (see Figure 1). Thus, downward moving electrons have positive pitch angle cosines; $0 < \mu \leq 1$. These electrons then travel through the plasma atmosphere undergoing collisions with the cold plasma particles and being adiabatically scattered by the converging B field. They thus change their pitch angle and energy and are allowed to return to the top of the atmosphere, then having negative pitch angle cosines. As the electrons can only diffuse from high to low energy and no process exists within our formulation for accelerating electrons to higher energies, the most convenient stepping parameter for the numerical analysis is the energy of the beam electron. The electron flux distribution is calculated over a three diminsional phase space (E,μ,τ) which is stratified into energy layers with each layer consisting of a grid in (μ,τ) space and being of constant value in energy space (see Figure A-1). The code generates the value of the electron flux at each grid point in a (μ,τ) plane of energy E_i from the given input fluxes at $\tau = 0$ and the flux values at the overlying (μ,τ) plane of energy $E_{i-1} > E_i$.

The input flux is specified at the top of the loop, $\tau = 0$, as a spectrum in energy and forward pitch angle, i.e., for the $0 < \mu \leq 1$ and $E < 1$ MeV half-plane. The flux values on the (μ,τ) grid corresponding to the largest electron energy are just the input fluxes specified at the top of the loop for that energy (1 MeV).

Once the flux values on one energy plane are calculated satisfactorily the code steps down one energy step to the next energy plane. The fluxes from the preceding plane just calculated are scaled for the new energy and, along with the specified input flux at that energy, a zeroth order (μ,τ) grid of fluxes is generated. The code then iterates over this energy plane until a satisfactory convergence of the flux values to those values satisfying equation (3) is found. A final n^{th} order (μ,τ) grid of electron fluxes is obtained which is stored as part of the results and is used to generate the zeroth order (μ,τ) grid for the next energy level down. Iteration on each (μ,τ) grid is obtained by sweeping down from the top of the atmosphere (τ=0) to the bottom and then returning to $\tau = 0$. The process is repeated until the results after each pair of sweeps have converged to within a prescribed error.

Boundary conditions can be imposed at the top to allow for electrons exiting with $\mu < 0$ to either be lost from the region of the calculations (simulating an open field configuration) or to be reflected back with positive μ's to simulate a closed field configuration symmetric at $\tau = 0$ (see Figure 1). Electrons with $\mu > 0$ at the bottom of the atmosphere are lost as are electrons which have their energy degraded to less than the minimum energy, which we have set at 10 keV.

B. Tests of the Numerical Results

In order to assess the accuracy of the code, we compare the numerical results with those of the analytic results described in §III. Note that some of the cases considered here have no physical meaning and serve solely as examples for which the analysis is tractable.

Case 1: If we set the coefficients C_1 and C_2 in equation (3) equal to zero and inject electrons with a pitch angle distribution $f_0(\mu) = -k\ln(1-\mu^2)$,

then, according to equation (7) we expect the pitch angle distribution to vary with depth in the form $f(\tau,\mu) = k(\bar{\tau} - \ln(1-\mu^2))$, that is, curves of $f(\tau,\mu)$ versus $-\ln(1-\mu^2)$ at constant $\bar{\tau}$, or depth, will be straight lines which are parallel for different depths and vertically positioned according to the value of $k\bar{\tau}$ at each depth. In Figure A-2 we have plotted our numerical evaluation of $f(\tau,\mu)$ against corresponding values of $-\ln(1-\mu^2)$ for several depths. As the electron's pitch angle is being affected adiabatically by the magnetic field, there is no energy dependence or energy loss in the process by which the electron beam evolves and, therefore, Figure A-2 is identical for all electron energies.

As can be seen from Figure A-2, the numerically evaluated $f(\tau,\mu)$ behaves exactly as expected throughout the atmosphere except at large depths where the difficulty of prescribing the injected flux in finite sized pitch angle bins for values of μ close to unity [where $-\ln(1-\mu^2)$ becomes very large] becomes evident.

Case 2a: If we now set $C_1 = 1$ and $C_2 = d\ln B/d\tau = 0$, we mimic a situation where the electrons lose energy by collisions within the atmosphere but do not change their pitch angle. If we inject a spectrum $\phi_0(E) = f_0(E)/\beta(E) = \eta^{-\delta} = [E^2/(E+1)]^{-\delta}$, i.e., a power law in η [recall that $\eta = E^2(E+1)$], then, according to equation (10), we expect the electron distribution to be described at each depth by $\phi(E,\mu,\tau) = (\tau/\mu + \eta)^{-\delta}$. In Figure A-3 we have plotted $\{\phi(E,\mu,\tau)^{-1/\delta} - \phi(E,\mu,0)^{-1/\delta}\}$ for three values of μ, versus depth τ and note that this should be independent of E and proportional to τ/μ. As is evident the numerical results agree perfectly with the expected analytic relation.

Case 2b: Finally, to check the accuracy of the treatment of diffusion in pitch angle we set $C_1 = d\ln B/d\tau = 0$, $C_2 = (3+\gamma)/4$ and inject into the atmosphere a beam with gaussian pitch angle distribution. Equation (14) describes the evolution of such a gaussian beam but is an approximation valid

at small pitch angles. Plotted against α^2, gaussian distributions at each depth, as given by equations (11) and (14), would be straight lines of slope $-1/(\alpha_o^2 + 4\bar{\tau})$, and these are shown as solid lines in Figure A-4 (for $\alpha_o^2 = 0.01$). The points and broken lines are the results from our numerical analysis at several depths τ. As can be seen, for small pitch angles the numerical results agree with the expected result to a high accuracy. Furthermore, as discussed in §IV, we note that the small pitch angle approximation is valid to larger angles than expected,especially at higher depths. At every depth the approximate analytic expression deviates from the numerical result only when the fluxes have dropped to less than one percent of the fluxes in the forward direction.

ACKNOWLEDGMENT

We would like to thank Dr. Gordon Emslie for a critical reading of the manuscript and for many valuable comments and discussions. We are also indebted to Drs. M. Walt, W.E. Francis and W.M. McDonald for providing us with the computer code which has formed the basis of our numerical work and for helpful discussions.

This work was supported by the National Aeronautics and Space Administration under Grant NSG 7092.

REFERENCES

Brown, J.C., 1972, Solar Phys., 26, 441.

Brown, J.C., Melrose, D.B. and Spicer, D.S., 1979, Ap.J., 228, 592.

Brown, J.C. and Smith, D.F., 1980, Rep. Prog. Phys., 41, 125.

Chubb, T.A., Kreplin, R.W. and Friedman, M., 1966, J. Geophys. Res., 71, 3611.

Datlowe, D.W. and Lin, R.P., 1973, Solar Phys., 32, 459.

Duijveman, A., Hoyng, P., and Ionson, J.A., 1981, Ap.J., in press.

Elcan, M.J., 1980, Ph.D. Thesis, U.C.S.D.

Emslie, A.G., 1978, Ap. J., 224, 241.

Emslie, A.G., 1980, Ap.J., 235, 1055.

Emslie, A.G., 1981a, Ap. J., submitted.

Emslie, A.G., 1981b, Ap. J., 244, in press.

Emslie, A.G. and Rust, D.M., 1979, Solar Phys., 65, 271.

Hoyng, P. et al, 1981, Ap. J. (Letters), in press.

Kane, S.R., 1974, in Coronal Disturbances, IAU Symp. 57, G. Newkirk, Jr. (ed.), p. 105.

Kindell, J.J. and Kennel, C.F., 1971, J. Geophys. Res., 76, 3055.

Knight, J.W. and Sturrock, P.A., 1977, Ap. J., 218, 306.

Lin, R.P. and Hudson, H.S., 1971, Solar Phys., 17, 412.

Marsh, K.A., Hurford, G.J., Zirin, H. and Hjellming, R.M., 1980, Ap.J., 242, 352.

Matzler, C., Bai, T., Crannell, C.J. and Frost, K.J., 1978, Ap. J., 223, 1058.

Petrosian, V., 1973, Ap. J., 186, 291.

Ramaty, R. and Lingenfelter, R.E., 1967, J. Geophys. Res., 72, 879.

Rosenbluth, M.N., McDonald, D.M. and Judd, D.L., 1957, Phys. Rev., 107, 1.

Smith, D.F. and Auer, L.H., 1980, Ap. J., 238, 1126.

Smith, D.F. and Lilliequist, G.G., 1979, Ap. J., 232, 582.

Sturrock, P.A., 1980, in Monograph from Skylab Solar Workshop II (Colorado Univ. Press).

Takakura, T., 1972, Solar Phys., 26, 151.

Walt, M., 1967, in Aurora and Airglow (Reinhold), B.M. McCormac (ed.), p. 287.

Walt, M., McDonald, W.M. and Francis, W.E., 1968, "Penetration of Auroral Electrons into the Atmosphere", in Physics of the Magnetosphere, ed. R. Carouillano and J.F. McClay, Reinhold, New York, p. 534.

FIGURE CAPTIONS

Figure 1. The two magnetic field structures that we consider. One is an open field structure with electrons injected (at $\tau = 0$) at some height above the photosphere with reflected electrons being allowed to leave freely once they reach $\tau = 0$ with $\mu < 0$. The other structure is the closed symmetric field structure where the electrons are injected at the top of the loop ($\tau = 0$) down towards the photosphere symmetrically in both directions. The electrons which return to $\tau = 0$ with $\mu < 0$ are then reflected back into the volume of positive τ to simulate the electrons crossings from one leg to the other.

Figure 2. The form of the electron flux pitch angle distribution at several depths in the atmosphere for a narrow injected beam (model 1) as obtained from the numerical results. Electrons with a pitch angle of zero degrees are streaming along the magnetic field lines downwards towards the photosphere; those with a pitch angle in excess of 90 degrees are moving upwards. The depths are scaled with the square of the electron energy as explained in the text. The inset shows a comparison of the numerically derived values (points) to those expected from the analytic expressions of equation (18) (solid lines).

Figure 3. The form of the electron flux energy spectrum at several depths in the atmosphere for model 1. At injection the beam has a flux spectrum of the form E^{-5} but low energy electrons lose energy by collisions faster than high energy electrons and are rapidly depleted in number within the atmosphere. The spectrum then develops a hump which moves to higher energies at greater depths according to $E^2_{max} = \tau/\delta$ as shown in the inset.

Figure 4. A comparison of the numerical results with the analytic expression of equation (22) at three energies. The upper diagram which is for energies of 30 and 70 keV uses the non-relativistic expressions for ζ which should be a good approximation at these energies. The lower diagram is for an electron energy of 750 keV and shows a comparison of the numerical results with two forms of equation (22), the lower one using the non-relativistic expression for ζ and the upper one using the relativistic expression for ζ.

Figure 5. The energy spectrum of the spatially integrated electron flux for three of our models: model 1 (our standard model); model 5 (which is the same as model 1 except that it has a harder injected electron energy spectrum); and model 9 (which is the most different from model 1 [see Table 1]). According to the analysis the total electron flux energy spectrum should have a particularly simple form as given by equation (24) and shown by the solid lines. The points represent the numerical results for the three models.

Figure 6. Same as Figure 2 , but for model 6.

Figure 7. The same as Figure 6 but for a beam which is isotropic in pitch angle at injection (model 7). Though the injected beam is not a gaussian, the form of the pitch angle spectrum at the two greatest depths is the same as those for models 1 and 6.

Figure 8. The electron energy spectrum at several depths in the atmosphere for model 9. As can be seen from Table 1, model 9 is most distinct from model 1 in terms of its parameters, yet, as a comparison with Figure 3 will show, model 9 retains the same basic form for the energy spectrum as model 1. This is to be expected as, for both models 1 and 9, the electron beam is primarily collisionally modified.

Figure A-1. A schematic respresentation of the three dimensional phase space of the electron number distribution. The phase space is stratified into (horizontal) energy planes, with each plane being a grid in pitch angle and depth within the atmosphere over which the electron number distribution is evaluated. The electron flux is specified over the positive pitch angle half of the $\tau = 0$ plane surface (shown shaded), the lower boundary being put at $\tau = \infty$ for which the number distribution is taken to be identically zero. The other half of the $\tau = 0$ surface (unshaded) corresponds to electrons with $\mu < 0$ at the top of the atmosphere, and these electrons can be either allowed to leave this region of phase space and lost from the calculation (open field configuration of Figure 1) or be reflected back into the region with $\mu > 0$ and added to the already specified injected flux (closed loop in Figure 1).

Figure A-2. The results of testing that part of the code handling the interaction of the electron beam with the converging magnetic field. The solid lines show $f(\mu,\tau)$ as given by equation (7) with $f_0(\mu) = -k\ln(1-\mu^2)$; the points represent the numerical results. The right hand side of the diagram is for downward travelling electrons, the left hand side for reflected electrons travelling upward. The depth parameter, $\bar{\tau}$, is related to the convergence of the magnetic field in the form $\bar{\tau} = \ln\{B(\tau)/B(0)\}$.

Figure A-3. The results of testing the part of the code describing the energy degradation only for electrons with pitch angle $\mu = 1.000$, $\mu = 0.9563$ and $\mu = 0.788$. The solid lines represent equation (9) for an injected electron spectrum $\phi_0(E,\mu,\tau) = (E^2/E+1)^{-\delta}$; the dots represent the numerical results.

Figure A-4. The results of testing that part of the code dealing with the diffusion of the electron's pitch angle by collisions for an injected gaussian pitch angle distribution. Note the excellent agreement between the numerical results (points) and the analytic expressions (solid lines) for small pitch angles.

John Leach
Institute for Plasma Research
Stanford University
Stanford, CA 94305
(415) 497-1276

Vahé Petrosian
Institute for Plasma Research
Stanford University
Stanford, CA 94305
(415) 497-1435

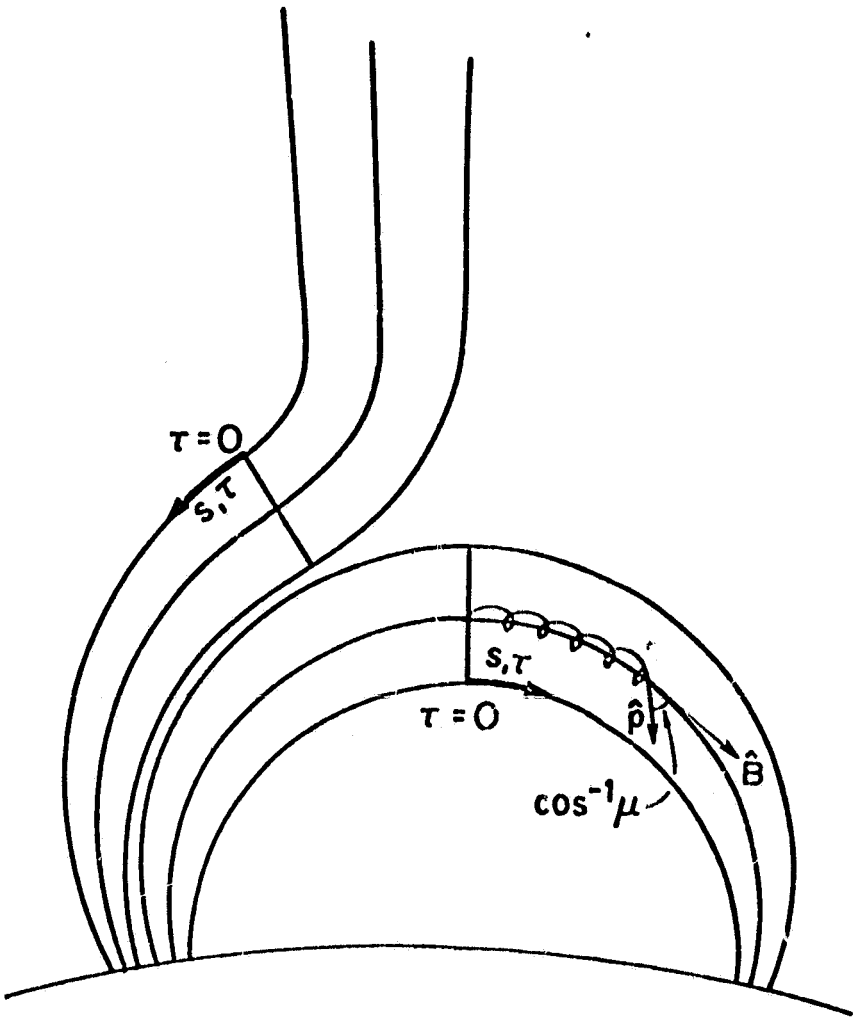
τ = 0
s,τ
s,τ
τ = 0
p̂
B̂
cos⁻¹μ

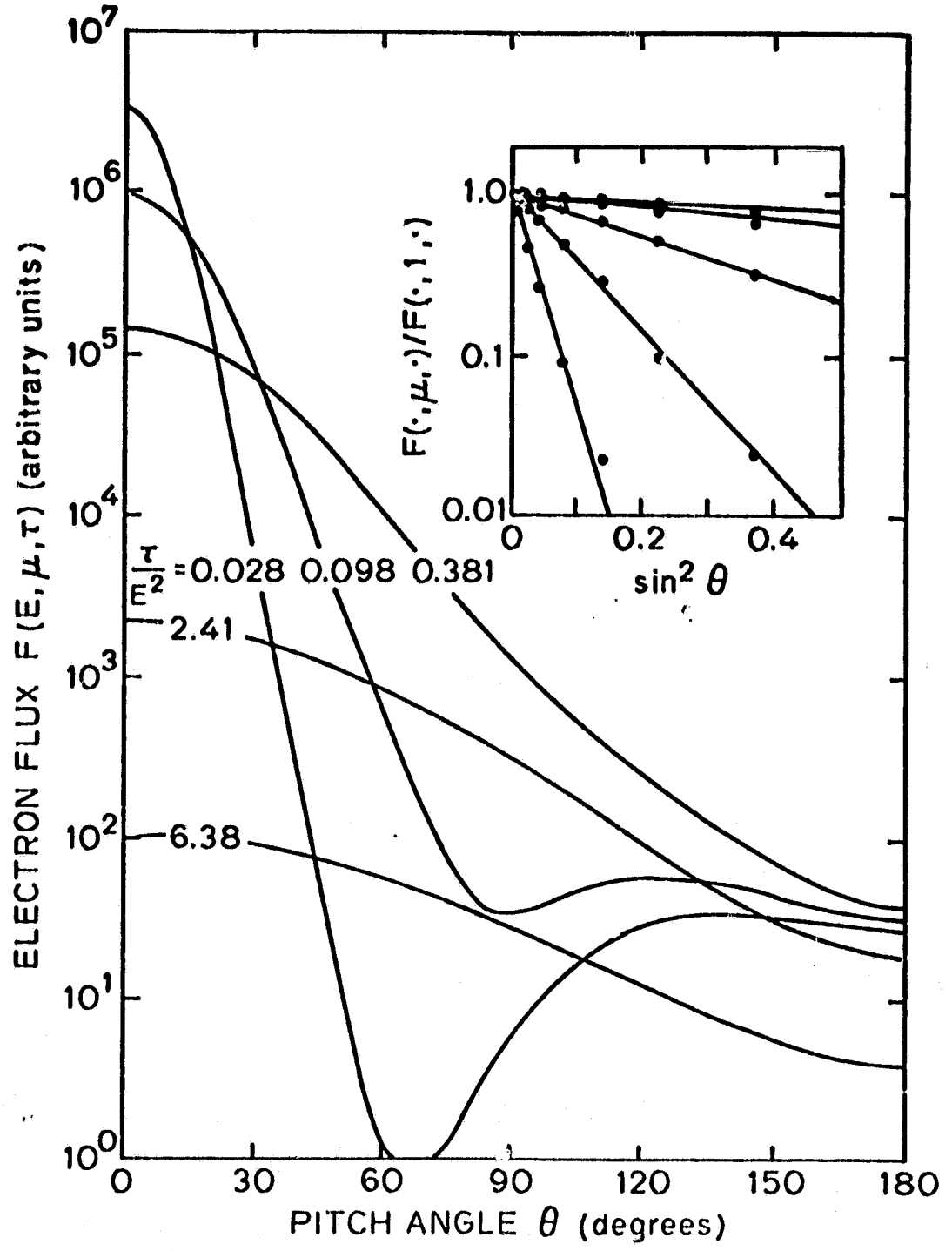
ELECTRON FLUX F(E, μ, τ) (arbitrary units)
PITCH ANGLE θ (degrees)
τ/E² = 0.028 0.098 0.381
2.41
6.38
F(·, μ, ·)/F(·, 1, ·)
sin² θ

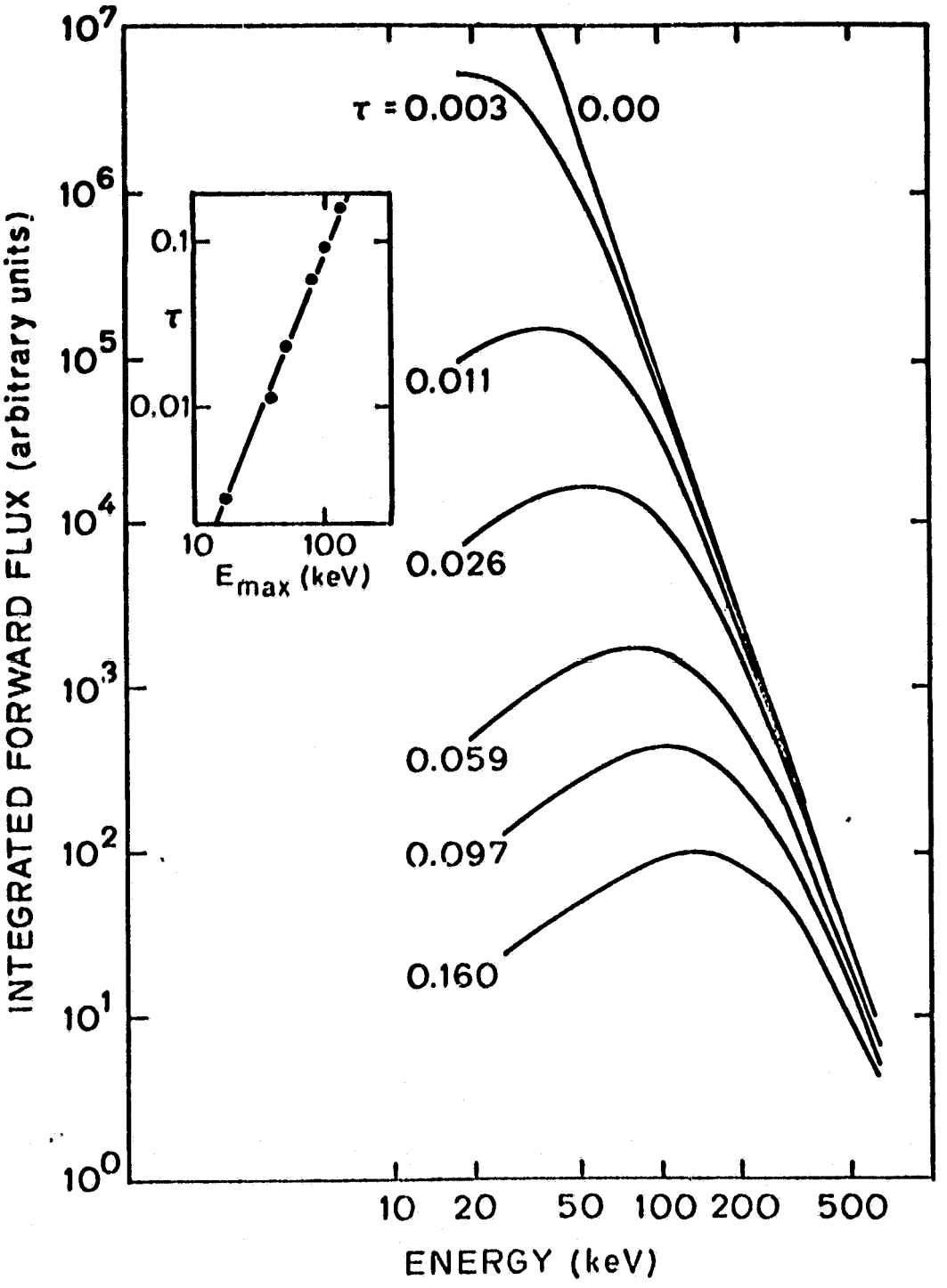
INTEGRATED FORWARD FLUX (arbitrary units)
10^7
10^6
10^5
10^4
10^3
10^2
10^1
10^0
τ = 0.003
0.00
0.011
0.026
0.059
0.097
0.160
0.1
τ
0.01
10
100
E_{max} (keV)
10 20 50 100 200 500
ENERGY (keV)

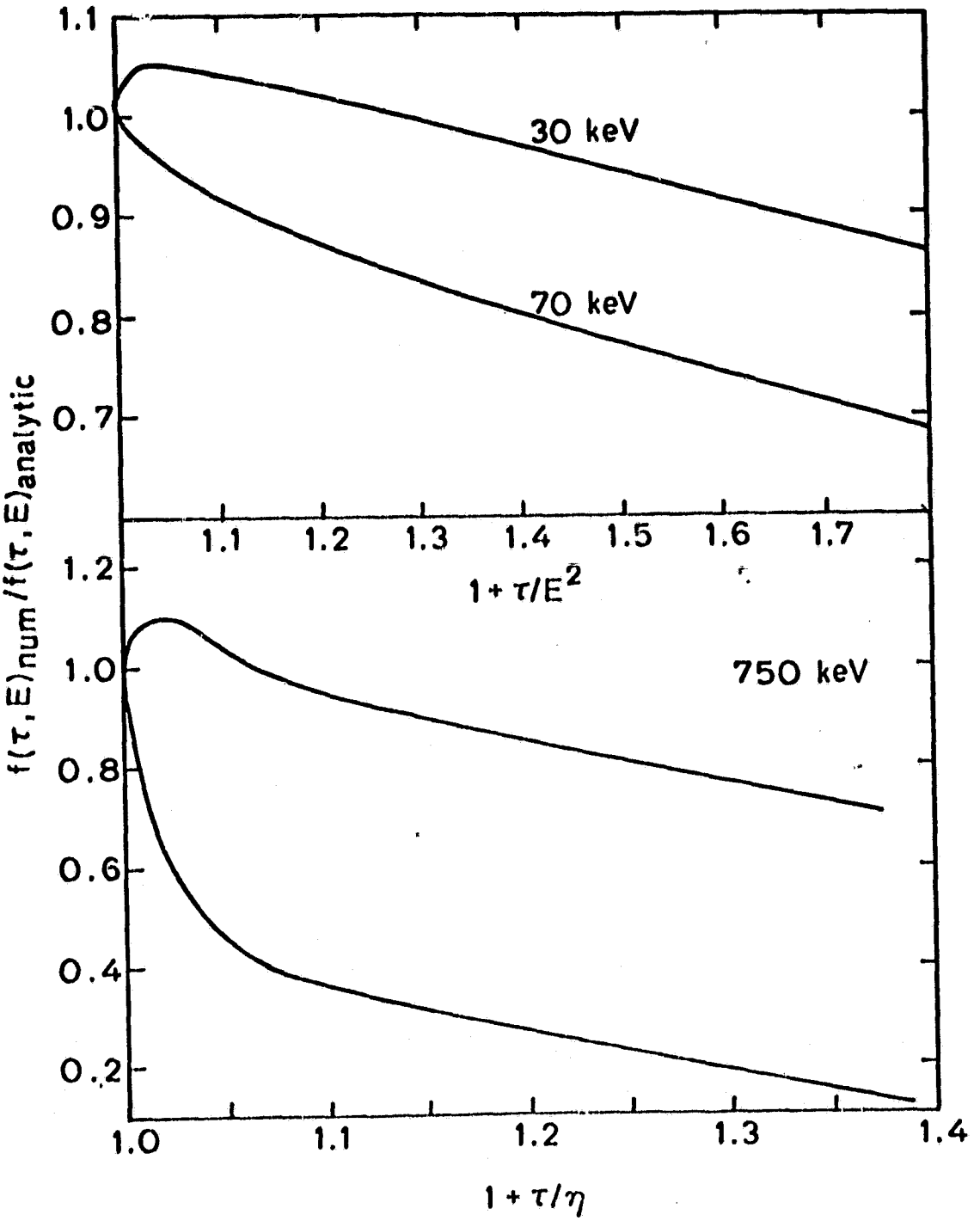
1.1
1.0
0.9
0.8
0.7
30 keV
70 keV
1.1
1.2
1.3
1.4
1.5
1.6
1.7
1 + τ/E²
1.2
1.0
0.8
0.6
0.4
0.2
750 keV
f(τ, E)num / f(τ, E)analytic
1.0
1.1
1.2
1.3
1.4
1 + τ/η

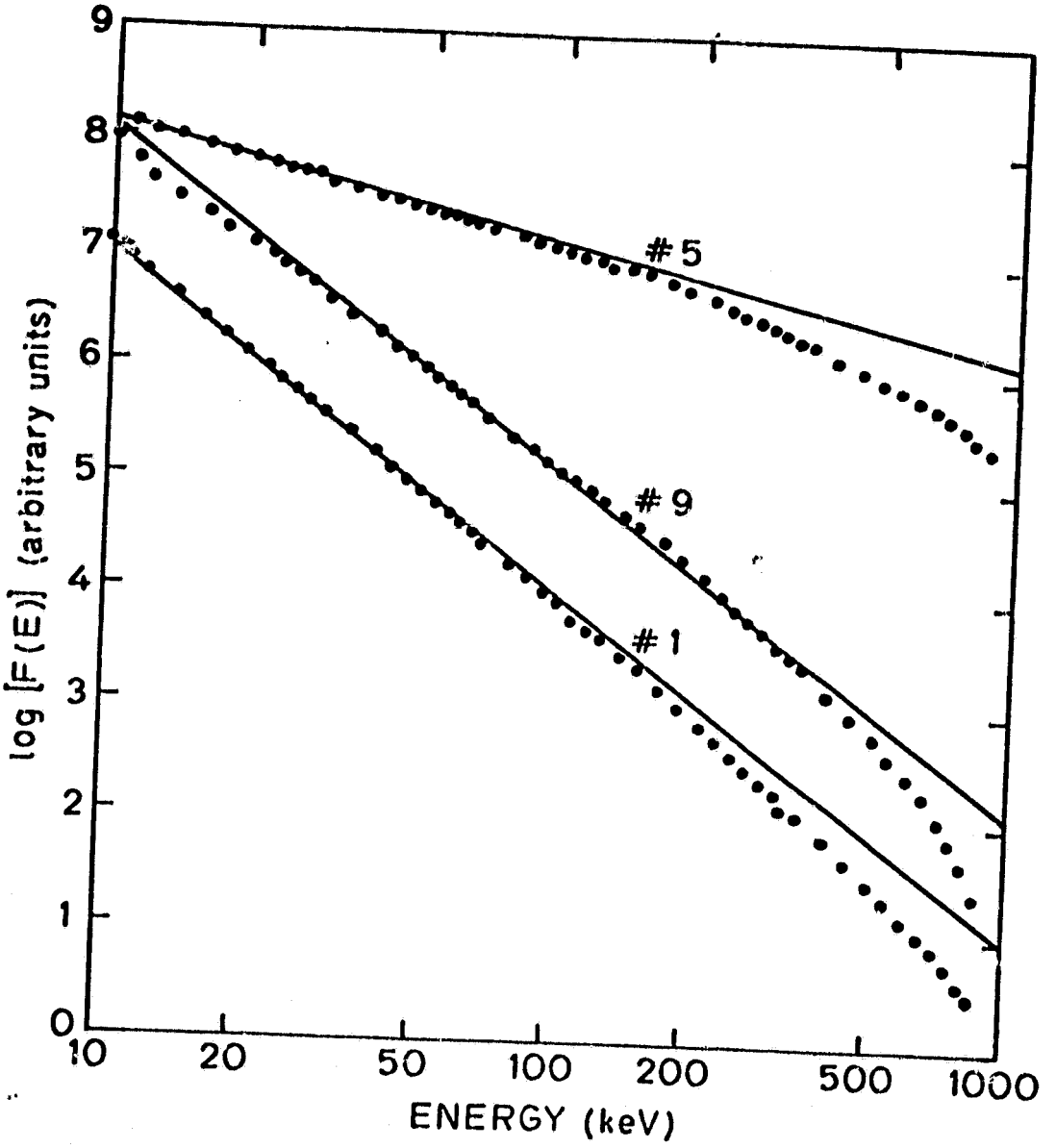
9
8
7
6
5
4
3
2
1
0
log [F(E)] (arbitrary units)
#5
#9
#1
10
20
50
100
200
500
1000
ENERGY (keV)

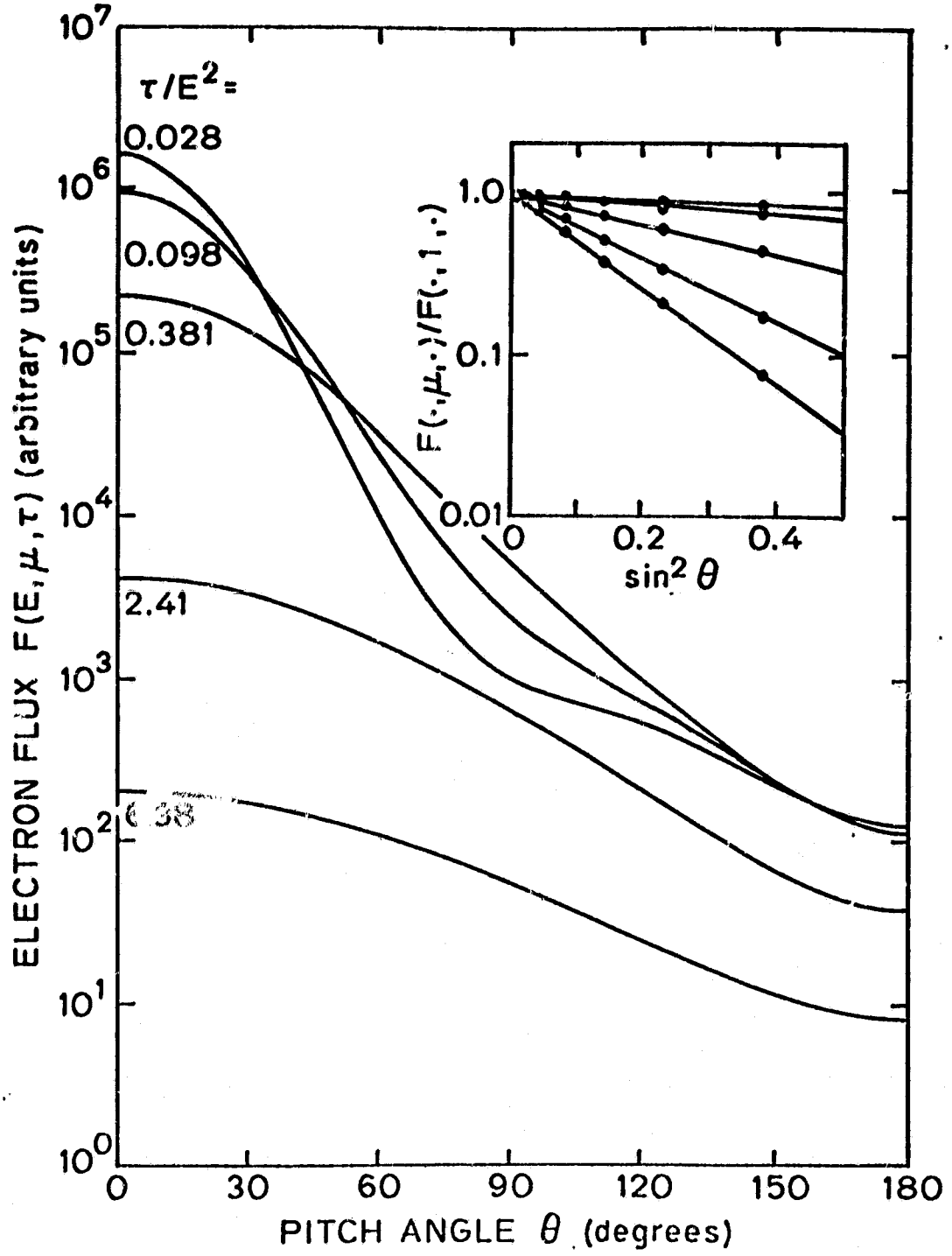
10^7
τ/E^2=
0.028
10^6
0.098
10^5
0.381
10^4
0.01
2.41
10^3
10^2
10^1
10^0
ELECTRON FLUX F(E, μ, τ) (arbitrary units)
0
30
60
90
120
150
180
PITCH ANGLE θ (degrees)
1.0
0.1
F(·, μ, ·)/F(·, 1, ·)
0
0.2
0.4
sin² θ

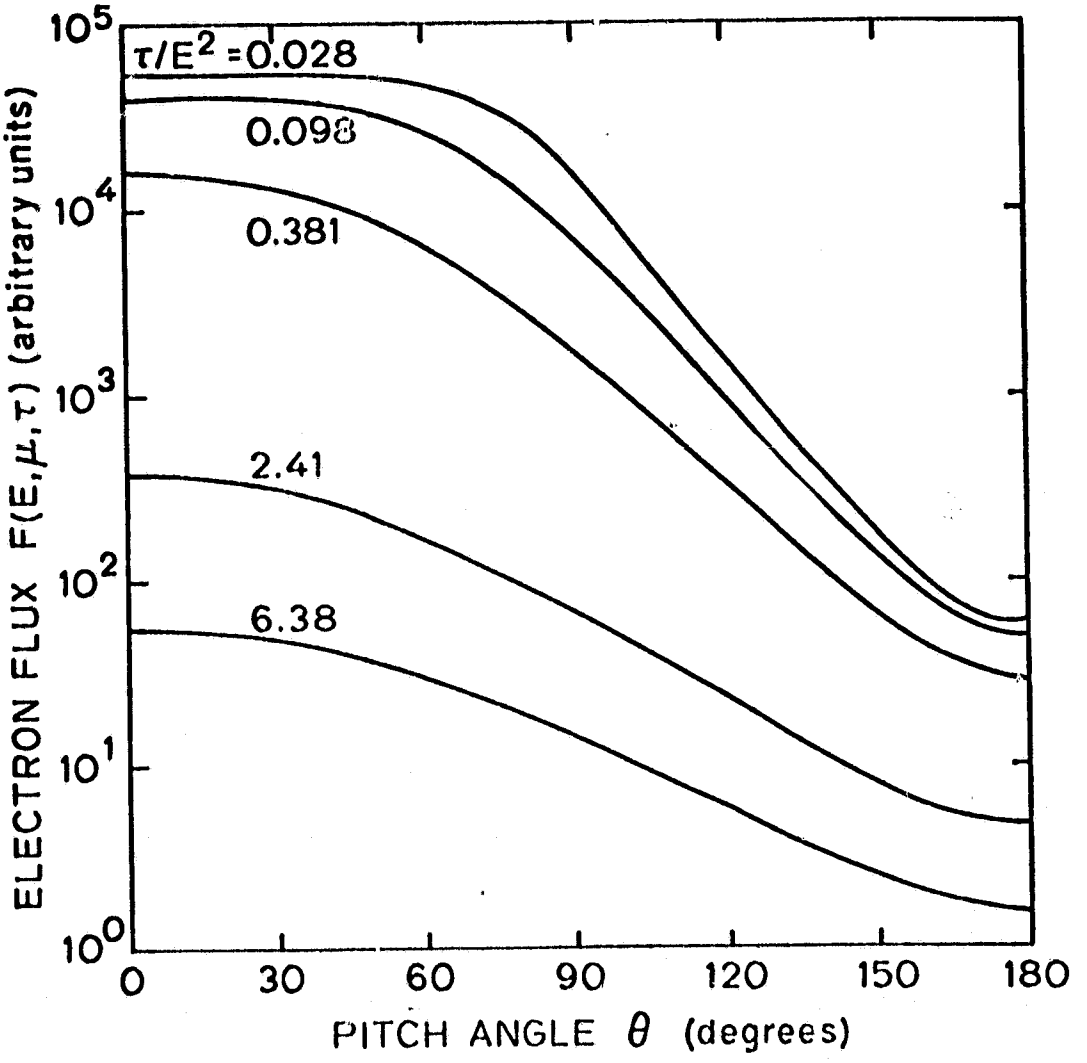
10^5
10^4
10^3
10^2
10^1
10^0
τ/E^2 =0.028
0.098
0.381
2.41
6.38
ELECTRON FLUX F(E,μ,τ) (arbitrary units)
0
30
60
90
120
150
180
PITCH ANGLE θ (degrees)

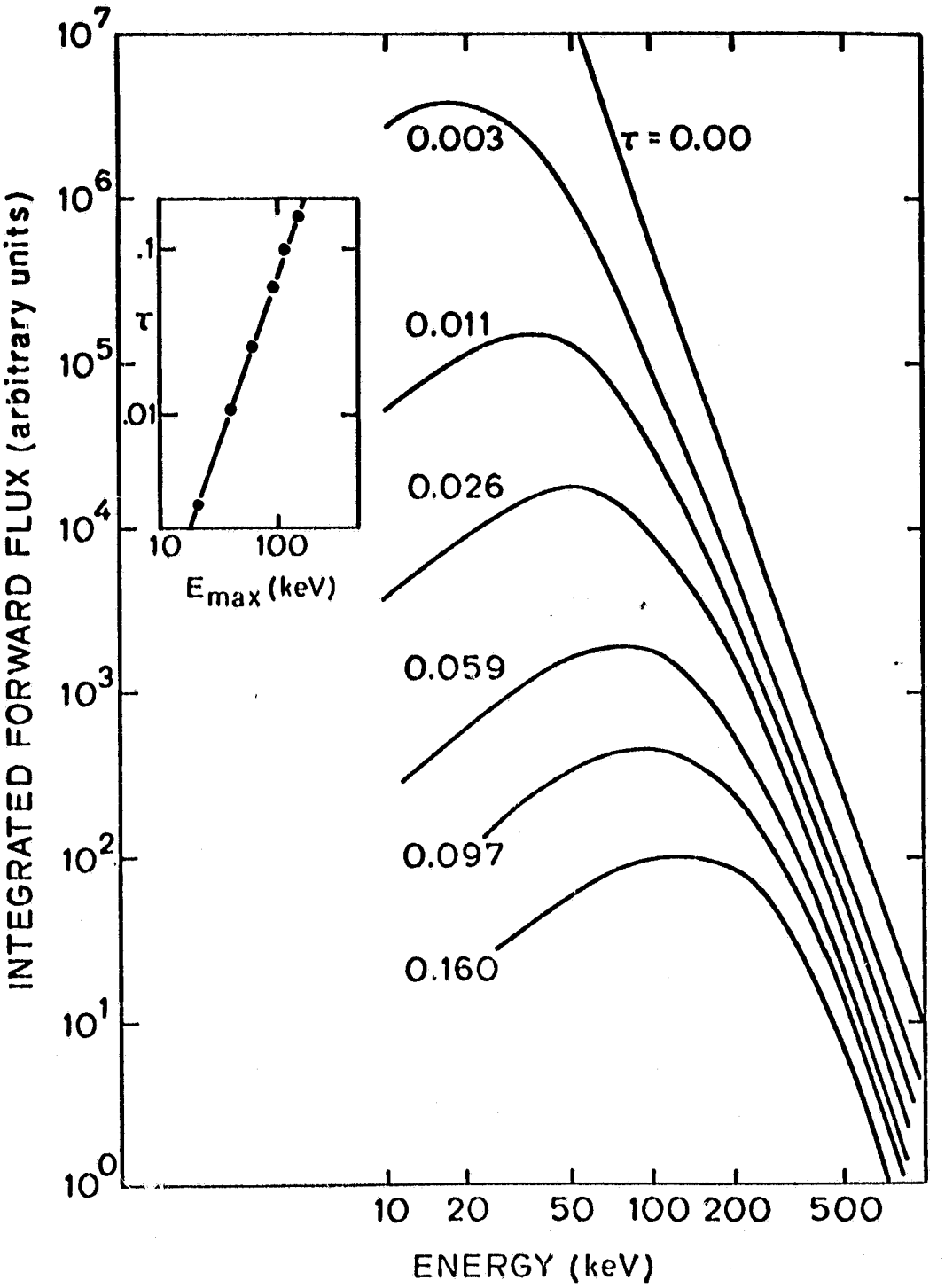
INTEGRATED FORWARD FLUX (arbitrary units)
10^7
10^6
10^5
10^4
10^3
10^2
10^1
10^0
0.003
τ = 0.00
0.011
0.026
0.059
0.097
0.160
τ
.1
.01
10
100
E_{max} (keV)
10 20 50 100 200 500
ENERGY (keV)

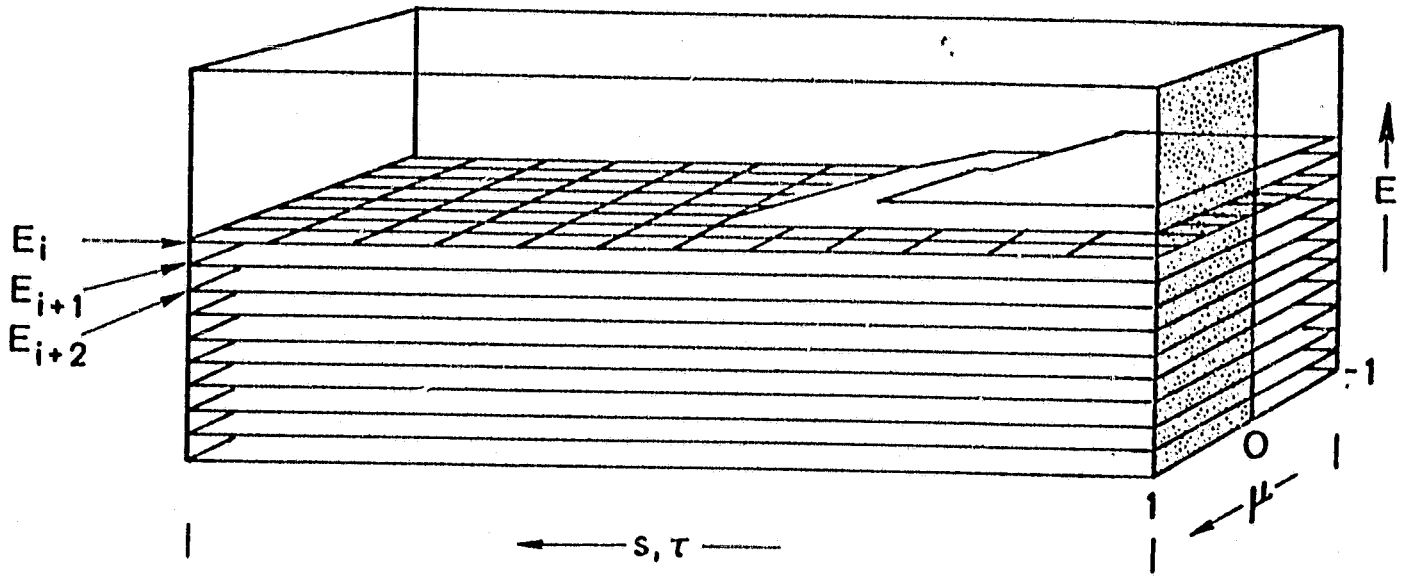
E_i
E_{i+1}
E_{i+2}
E
-1
0
1
μ
s, τ

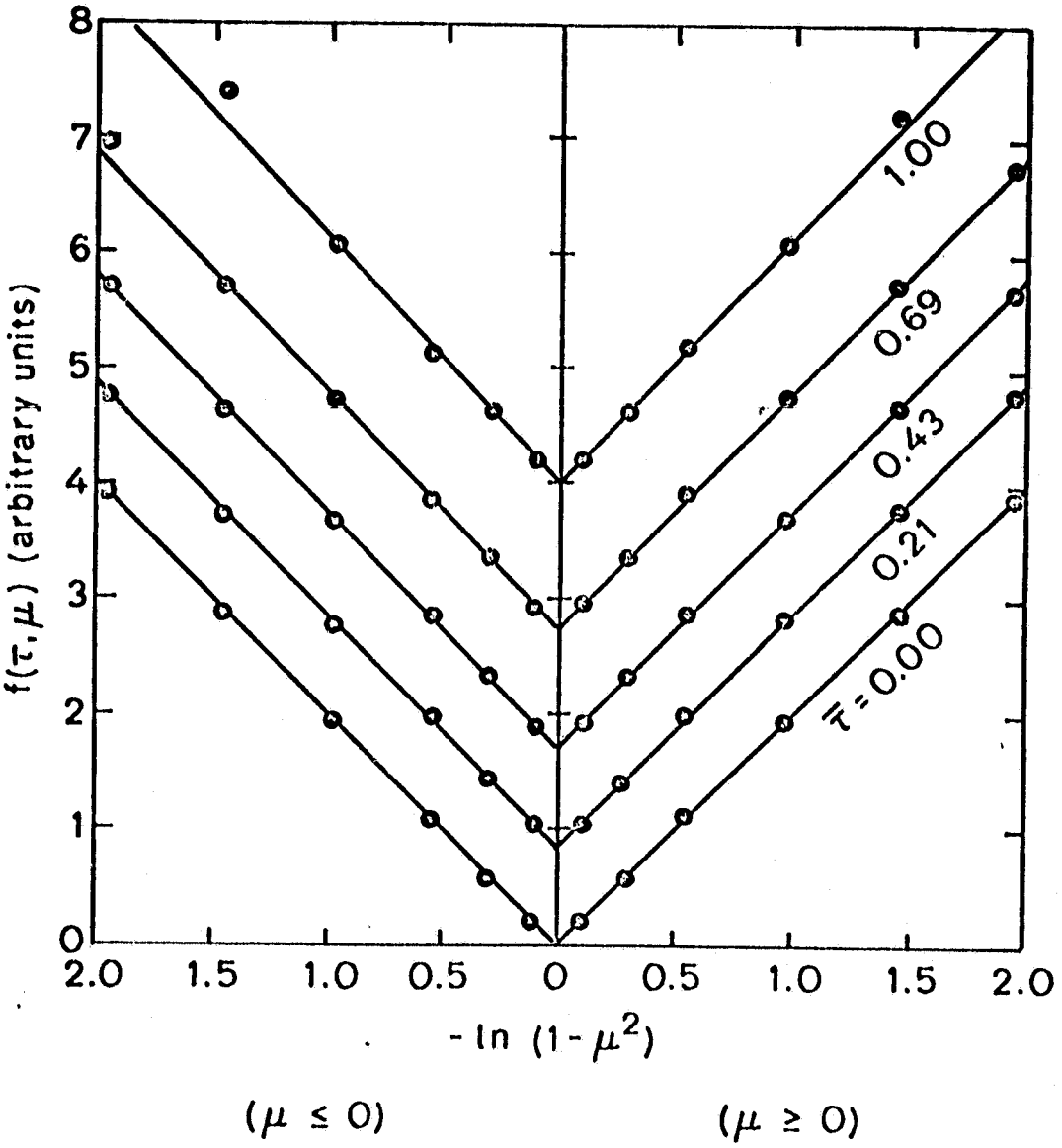
8
7
6
5
4
3
2
1
0
f(τ, μ) (arbitrary units)
2.0
1.5
1.0
0.5
0
0.5
1.0
1.5
2.0
- ln (1 - μ²)
1.00
0.69
0.43
0.21
τ = 0.00
(μ ≤ 0)
(μ ≥ 0)

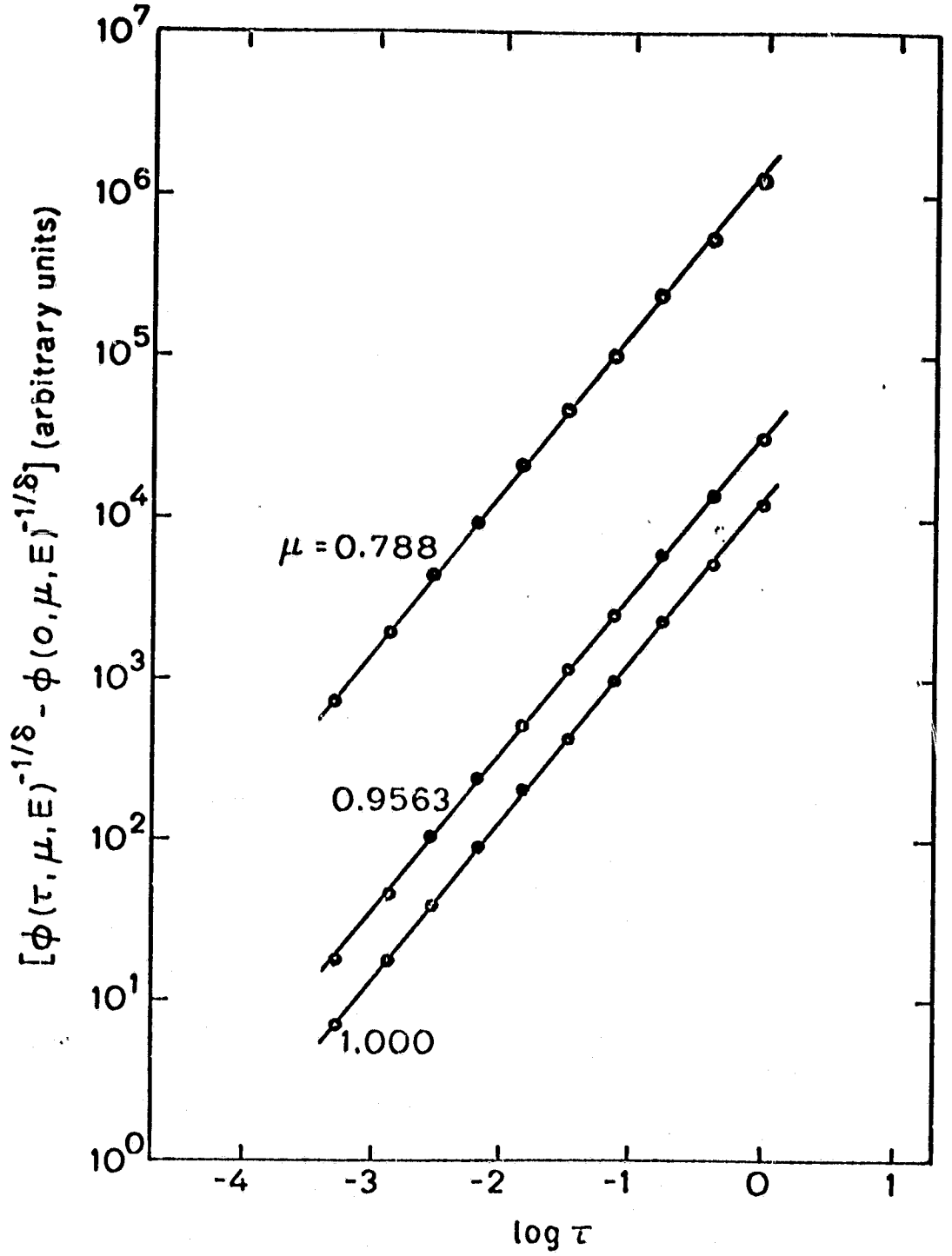
10^7
10^6
10^5
10^4
10^3
10^2
10^1
10^0
$[\phi(\tau,\mu,E)^{-1/\delta} - \phi(0,\mu,E)^{-1/\delta}]$ (arbitrary units)
$\mu = 0.788$
0.9563
1.000
-4
-3
-2
-1
0
1
log τ

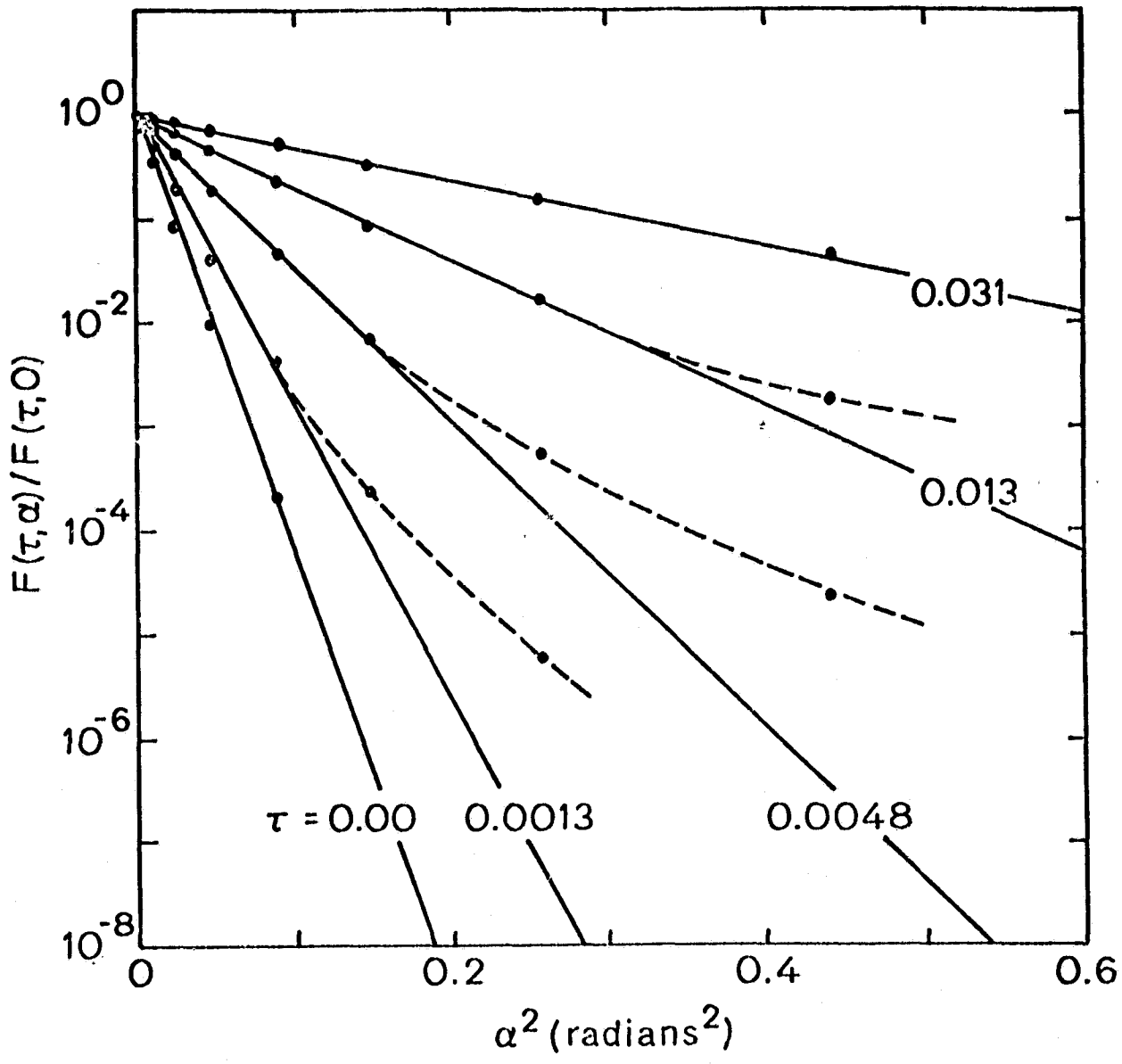
10^0
10^{-2}
10^{-4}
10^{-6}
10^{-8}
$F(\tau,\alpha)/F(\tau,0)$
0.031
0.013
τ = 0.00
0.0013
0.0048
0
0.2
0.4
0.6
α^2 (radians^2)